Electronic structure of V_2O_5: Role of octahedral deformations

V. Eyert*
Hahn-Meitner-Institut, Theory Department, Glienicker Straße 100, D-14109 Berlin, Germany

K.-H. Höck
Institut für Physik, Universität Augsburg, Memminger Straße 6, D-86135 Augsburg, Germany
(Received 12 December 1997; revised manuscript received 27 January 1998)

We present results of all-electron electronic-structure calculations for semiconducting vanadium pentoxide. The calculations are based on density-functional theory within the local-density approximation and employ the augmented spherical wave method in its scalar-relativistic implementation. The electronic properties are modified significantly by strong hybridization between O $2p$ and crystal field split V $3d$ states. Strong deviations of the VO_6 octahedra from cubic coordination give rise to the narrow split-off conduction band as a characteristic feature of V_2O_5. Furthermore, we demonstrate that distortions of the octahedra along the crystallographic c axis drastically increase the bonding-antibonding splitting of the V $3d_{xz}/3d_{yz}$ derived bands, whereas distortions perpendicular to the c axis reduce the bandwidth of the split-off V $3d_{xy}$ bands. Both effects contribute to the stability of V_2O_5 and enhance the optical band gap. [S0163-1829(98)12919-3]

I. INTRODUCTION

The transition-metal oxides attract a lot of attention due to their interesting physical and chemical properties, which arise from the narrow d states and their hybridization with the ligand p orbitals. Among this large class of materials, the vanadium-oxygen system arouses special interest. Although made up of only two constituents, the vanadium-oxygen phase diagram contains several stoichiometric compounds and a broad spectrum of physical phenomena could be studied.[1]

Some of the vanadium oxides undergo reversible metal-insulator transitions as a function of temperature, pressure, or doping, which come along with magnetic transitions and/or structural changes. Prominent examples are VO_2 and V_2O_3, where the change in resistivity extends over several orders of magnitude.[2] In both compounds, the first-order phase transition is accompanied by structural changes affecting the geometry of the characteristic VO_6 octahedra.[1] In addition, V_2O_3 exhibits long-range antiferromagnetic order below the transition temperature.[2] The origin of the metal-insulator transition, however, is still a matter of controversy. Several models have been proposed ranging from models stressing the importance of electron-phonon coupling to such favoring strong electron-electron correlations as the driving force. As a consequence, a complete and accepted picture of the physics of the vanadium oxides has not yet evolved.

In an attempt to split the aforementioned problem of identifying the predominant physical mechanisms into subproblems, which might be easier to attack, it is worthwhile to study related compounds where, for instance, electron-electron correlations are regarded as playing a minor role. One such system is vanadium pentoxide, which is a semiconductor at all temperatures without exhibiting a phase transition.[1,3] At the same time, the crystal structure of V_2O_5 shows distinct deformations of the VO_6 octahedra, some of which are equivalent to those present in VO_2 and V_2O_3. Hence, by investigating V_2O_5, we might be able to shed some light on the influence of these structural peculiarities on the electronic structure without being blinded by electron-electron correlations.

For some time, V_2O_5 has been the subject of intense work because of its small and highly anisotropic n-type electrical conductivity.[1,3,4] The anisotropy was related to the peculiarities of the crystal structure: the atoms form double chains within planes that are separated by a van der Waals gap.[5–8] From the Hall effect, thermopower, and EPR measurements, Ioffe and Patrina concluded that the reduced conductivity, in contrast, can be attributed to the formation of small polarons.[9] According to optical-absorption measurements, the fundamental absorption edges amount to 2.15, 2.17, and 2.22 eV for $E\|a$, $E\|b$, and $E\|c$, respectively.[10] From optical reflectance measurements, Mokerov *et al.* concluded that the optical properties for energies between 2.2 and 8–9 eV are dominated by transitions from oxygen $2p$ to vanadium $3d$ states, whereas above 8–9 eV the transitions are to the vanadium $4s$ states.[11] These authors reported that the fundamental absorption is due to a band of only 0.4 eV width, located at about 2.5 eV above the highest occupied states. In addition, they found a second absorption edge at an energy above 2.6 eV.[11] Their finding of a low energy split-off conduction band provided a different clue to the understanding of the low carrier mobility.

These findings were confirmed by photoemission experiments using UPS, XPS, XAS, and Auger electron spectroscopy.[12–18] According to Zhang and Henrich, the valence band of about 5.5 eV width divides mainly into three peaks.[15] The two lower peaks are due to the V-O bonding, whereas the highest peak corresponds to nonbonding O $2p$ orbitals. In addition, these authors found considerable changes of UPS spectra taken before and after XPS measurements on the (001) surface, which, in particular, affected the two strong-binding valence-band peaks and which they attributed to the tendency of V_2O_5 to form defects and to undergo transitions to other oxides.[15]

In the past years, V_2O_5 has attracted renewed interest as a

starting material for the intercalation of alkaline atoms into the van der Waals gap. Attention was focused, in particular, on the stoichiometric sodium intercalation system α'-NaV_2O_5, where the sodium atoms form ordered chains within the van der Waals gap[19] and which exhibits a spin-Peierls transition at $T_{SP}=33.5$ K.[20–26]

Theoretical work on V_2O_5 comprises semiempirical tight-binding and non-self-consistent first principles calculations as well as self-consistent calculations for clusters near the (001) surface.[27–31] However, a state-of-the-art first principles study of the bulk material is still missing. In order to fill this gap, we initiated the present study. In doing so, we aim in particular at a comprehensive analysis of the electronic structure in terms of a few relevant orbitals. Nevertheless, for a detailed investigation of the mechanisms that cause the characteristic octahedral deformations, it is not sufficient to stay with only the experimentally determined crystal structure. For this reason, we extended our study to calculations for V_2O_5 with hypothetical crystal structures in which ideal octahedral geometry was gradually restored. The resulting changes of the electronic structure allow us to deduce detailed information concerning the stability of the actual crystal structure. Finally, we complement the electronic properties with a discussion of the chemical bonding by evaluating the crystal orbital overlap population (COOP),[32] which was recently implemented into the augmented spherical wave (ASW) method.[33]

A brief account of the present results has been given recently,[34–36] whereas a detailed comparison with angle-resolved photoemission data will be published in the near future.[37] The paper is organized as follows. Starting with a short summary of the crystal structure data in Sec. II, we outline the calculational method in Sec. III. The results are presented in Sec. IV. The conclusion, Sec. V, sums up the most important findings.

II. CRYSTAL STRUCTURE

V_2O_5 crystallizes in a simple orthorhombic (so) lattice with space group $Pmmn$ (D_{2h}^{13}) and lattice constants $a=11.512$ Å, $b=3.564$ Å, and $c=4.368$ Å.[8] The primitive cell comprises two formula units. We display the crystal structure in Fig. 1, where we also indicate the three different types of oxygens. They are usually designated as vanadyl (O_v), chain (O_c), and bridge (O_b) oxygens. The positions of the atoms and the crystal structure parameters are listed in Table I, where the Wyckoff positions ($2a$) and ($4f$) are special cases of the general position ($8g$): $\pm(x,y,z)$, $\pm(x,\frac{1}{2}-y,z)$, $\pm(\frac{1}{2}-x,y,z)$, $\pm(\frac{1}{2}-x,\frac{1}{2}-y,z)$.

The crystal structure consists of alternating (horizontal) layers, which contain either vanadium, chain, and bridge oxygen atoms or, alternatively, vanadyl oxygen atoms. Within the first type of layers, vanadium and chain oxygen atoms form double zigzag chains along the $\langle 010\rangle$ direction, which, within the planes, are connected via the bridge oxygen atoms. The vanadyl oxygen atoms, finally, are located just below and above the vanadium atoms: thus the vanadium atoms reside near the centers of VO_6 octahedra formed by one bridge, two vanadyl, and three chain oxygen atoms. These octahedra share edges via the chain oxygens and corners via the bridge oxygens.

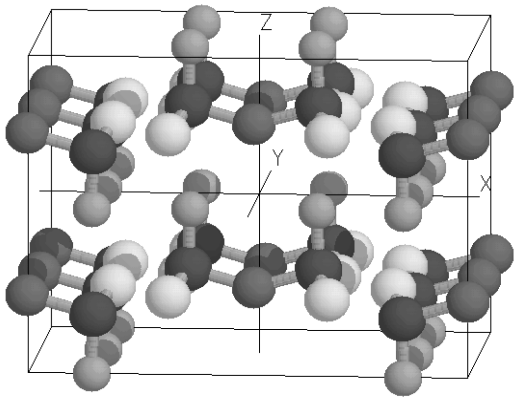

FIG. 1. Crystal structure of V_2O_5. Lines parallel to the x, y, and z axes mark the a, (double) b, and (double) c orthorhombic axes. Vanadium atoms are printed in black. Vanadyl, chain, and bridge oxygens are shaded medium, light, and dark gray, respectively.

Still, the vanadium atoms experience distinct displacements away from the centers of the octahedra. First, the vanadium and the vanadyl oxygen atoms move vertically towards each other. One short (1.577 Å) and one long (2.791 Å) V-O_v distance evolves, and the interaction along the latter reduces to rather weak van der Waals forces. This fact explains the observed easy cleavage of V_2O_5 crystals parallel to the (ab) layers.[1] Second, the vanadium and the chain oxygen atoms experience shifts parallel to the x axis towards the bridge oxygen atoms. This leads to the zigzag shape of the $\langle 010\rangle$ double chains. The resulting in-plane distances within the octahedra amount to 1.779 Å for the V-O_b bond and 1.878 Å and 2.017 Å for the V-O_c bonds parallel to the y and x axis, respectively. Due to these displacements, the remaining basic units finally become VO_5 pyramids rather than regular octahedra.

III. CALCULATIONAL DETAILS

Our calculations are based on density-functional theory (DFT) and the local-density approximation (LDA).[38,39] We employ the augmented spherical wave (ASW) method[40] in its scalar-relativistic implementation[41,42] (see Refs. 43 and 44 for more recent descriptions). Since the ASW method uses the atomic sphere approximation (ASA),[45] we had to insert so-called empty spheres into the open crystal structure of V_2O_5. These empty spheres are pseudoatoms without a nucleus, which are used to model the correct shape of the crystal potential in large voids.[46] In order to minimize the sphere overlap, we have recently developed the algorithm described in Appendix A, which solves the problem of finding optimal empty sphere positions as well as radii of all

TABLE I. Crystal structure parameters.

Atom	Wyckoff positions	Parameters		
		x	y	z
V	($4f$)	0.10118	0.25	−0.1083
O_v	($4f$)	0.1043	0.25	−0.469
O_c	($4f$)	−0.0689	0.25	0.003
O_b	($2a$)	0.25	0.25	0.001

TABLE II. Empty sphere positions.

Atom	Wyckoff positions	Parameters x	y	z
E_1	$(4f)$	−0.38	0.25	0.5
E_2	$(2b)$	−0.25	0.25	0.1389
E_3	$(2a)$	0.25	0.25	0.4208
E_4	$(8g)$	0.0217	0.0595	0.2533
E_5	$(8g)$	0.1561	0.0238	0.1672

spheres automatically. By inserting 24 empty spheres into the simple orthorhombic unit cell of V_2O_5, we kept the linear overlap of any pair of physical spheres below 18%, and the overlap of any pair of physical and empty spheres below 24%. The positions of the empty spheres are listed in Table II. In addition to the empty sphere positions, the algorithm proposed atomic sphere radii for all spheres, which are listed in Table III. Table III moreover supplies the orbitals used as the basis set for the present calculations. States given in parentheses were included as tails of the other orbitals (see Refs. 40, 43, and 44 for more details on the ASW method).

The Brillouin zone sampling was done using an increased number of **k** points ranging from 27, 64, 216, to 512 points within the irreducible wedge, ensuring convergence of our results with respect to the fineness of the **k** space grid. Self-consistency was achieved by an efficient algorithm for convergence acceleration;[47] the convergence criterion for the atomic charges and the total energy was 10^{-8} electrons and 10^{-8} Ry, respectively.

In addition to the band structure and the (partial) densities of states, we evaluated the crystal orbital overlap population (COOP). This concept has been introduced by Hoffmann[32] in order to allow for a discussion of chemical bonding. The evaluation of the COOP has been recently implemented in the ASW method (see Refs. 33 and 34 for details); it was successfully applied to the interpretation of bonding properties of various compounds.[34]

IV. RESULTS AND DISCUSSION

A. Electronic structure and density of states

To the first approximation, the semiconducting ground state of V_2O_5 may be understood within an ionic picture where the O $2p$ orbitals are completely filled (O^{2-}), whereas the V $3d$ states are unoccupied (V^{5+}, $3d^0$). From the nearly

TABLE III. Atomic sphere radii and basis set orbitals.

Atom	Radius/a_B	Orbitals				
V	1.965	$4s$	$4p$	$3d$	$(4f)$	
O_v	1.521	$2s$	$2p$	$(3d)$		
O_c	2.079	$2s$	$2p$	$(3d)$		
O_b	1.680	$2s$	$2p$	$(3d)$		
E_1	2.598	$1s$	$2p$	$3d$	$4f$	$(5g)$
E_2	2.583	$1s$	$2p$	$3d$	$(4f)$	
E_3	2.516	$1s$	$2p$	$3d$	$4f$	$(5g)$
E_4	1.532	$1s$	$(2p)$			
E_5	1.613	$1s$	$(2p)$			

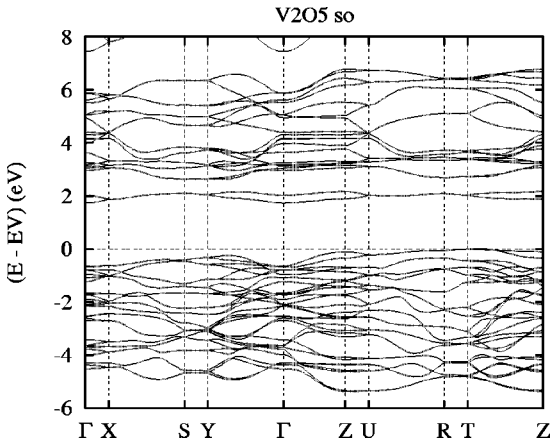

FIG. 2. Electronic bands of V_2O_5 along selected symmetry lines within the first Brillouin zone of the simple orthorhombic lattice, Fig. 3. Energies are given relative to the valence-band maximum E_V.

octahedral surrounding of the vanadium ions, we would furthermore expect that crystal field splitting leads to t_{2g} states at the lower edge of the conduction band, while the e_g bands are located at higher energies. Due to strong deviations from octahedral coordination, however, all orbitals will finally split into singlets. Nevertheless, in the present context these rather schematic considerations just serve as a framework for further discussions.

We display in Fig. 2 the electronic states along selected high symmetry lines within the first Brillouin zone of the simple orthorhombic lattice, Fig. 3. The corresponding density of states (DOS) is given in Fig. 4, where we have added the dominant partial densities of states. Not shown are low-lying oxygen $2s$ states.

In general, the bands shown in Fig. 2 reflect the anisotropies of the crystal structure. Obviously, there exists only a small dispersion along the direction Γ-X, which is the in-plane direction perpendicular to the V-O_c chains. In contrast, we observe larger dispersions along Γ-Y, i.e., parallel to the double chains. For the direction Γ-Z the dispersion arises distinctly for different bands. Whereas the conduction bands below 4.5 eV display hardly any dispersion, the valence bands as well as the higher conduction bands have a dispersion similar to that along Γ-Y.

In Figs. 2 and 4 we identify three groups of bands. The valence band starts at ≈ -5.5 eV below the valence-band maximum and consists of 30 bands that trace back mainly to O $2p$ states but have a non-negligible contribution due to the V $3d$ states. Bands are most easily counted along the line X-S where they are twofold degenerate.

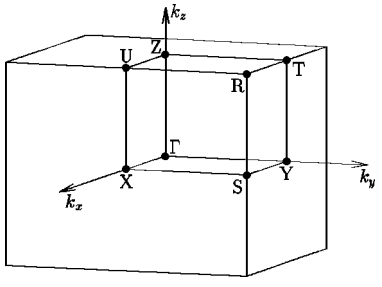

FIG. 3. First Brillouin zone of the simple orthorhombic lattice.

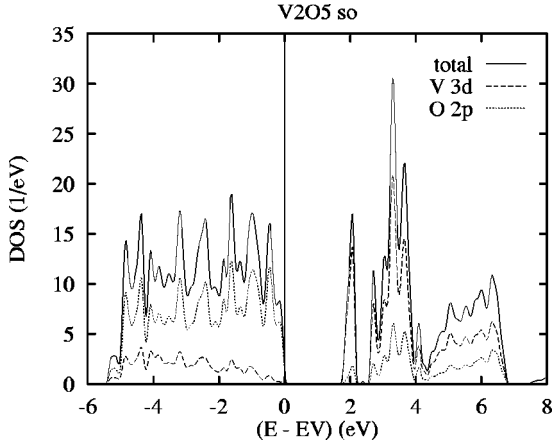

FIG. 4. Total and partial densities of states (DOS) of V_2O_5. Here and in the following figures, partial DOS include all atoms of a species.

Above the band gap we find, in good agreement with the experimental data of Mokerov *et al.*,[11] a narrow conduction band of only 0.45 eV width that is separated from the broad higher conduction band by an additional gap of ≈0.35 eV. Whereas this so-called split-off band comprises two single bands, the high energy region consists of 18 bands. Both groups originate mainly from the vanadium 3*d* orbitals, but again we observe in Fig. 4 a substantial *p*-*d* hybridization especially for the upper conduction band. The vanadium 4*s* derived bands are visible at the top of Fig. 2. All other states that are not included in Fig. 4 play only a negligible role in the given energy interval.

The valence and conduction band are separated by an indirect optical band gap with the band extrema located near the T and Γ point, respectively. The calculated size of the gap of ≈1.74 eV is smaller than the experimental value of ≈2.2 eV.

B. Partial DOS

Despite the strong distortions of the oxygen octahedra centered around the vanadium atoms, the dominant splitting of the V 3*d* states results from the cubic part of the crystal field. This is demonstrated in Fig. 5, where we display the partial V 3*d* density of states together with the contributions

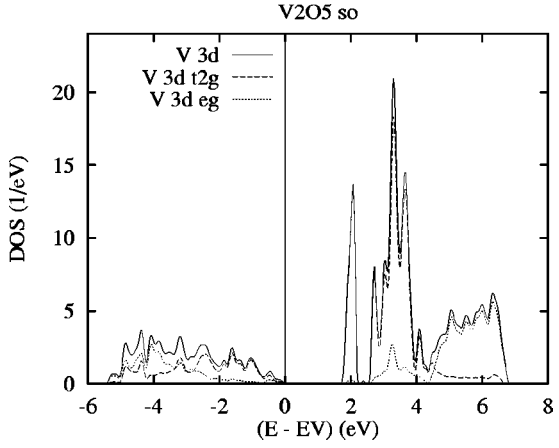

FIG. 5. Partial V 3*d* DOS of V_2O_5.

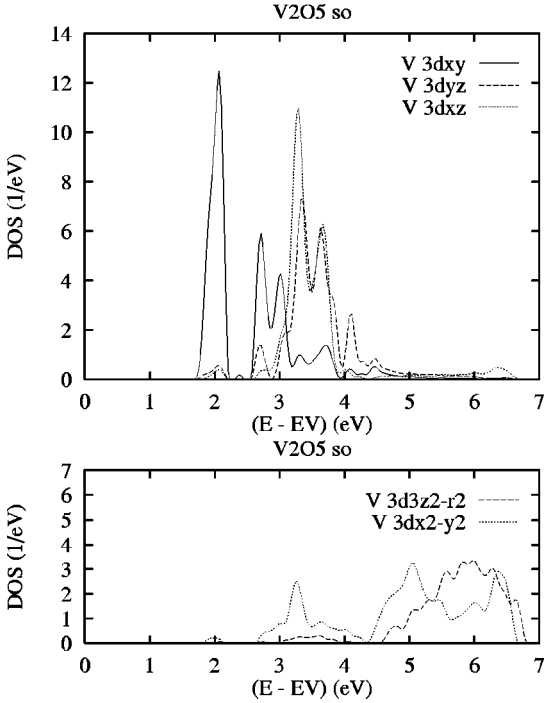

FIG. 6. Partial V 3*d* t_{2g} and e_g DOS of V_2O_5.

from the t_{2g} and e_g orbitals. In the conduction band we observe an almost complete separation of these two groups. The t_{2g} states appear almost exclusively in the energy range from ≈1.74 to ≈4.5 eV, whereas the e_g states dominate at higher energies. The small but finite t_{2g}-e_g configuration mixing is a measure of the octahedral distortion, which reduces the local symmetry at the V sites to monoclinic (C_{1h}). The aforementioned reduced dispersion of the conduction bands below 4.5 eV is reflected by the higher density of states of the t_{2g} states. It is a consequence of the smaller overlap with the ligand 2*p* states via π bonds. The e_g states, in contrast, form σ bonds with the oxygen 2*p* states, and thus exhibit a larger overlap and hence a stronger dispersion of the bands as well as a larger bonding-antibonding splitting. The latter becomes obvious from the vanadium contributions to the density of states of the valence band, where the e_g states lie below the t_{2g} states. Although the energetical separation of the t_{2g} and e_g manifolds is not as complete as for the conduction bands, we clearly identify a change of the dominating V 3*d* character at ≈−3 eV.

We display in Fig. 6 the partial DOS of the V 3*d* t_{2g} and e_g states resolved into their symmetry components. We concentrate especially on the conduction bands. Due to the substantial hybridization of the V 3*d* with the O 2*p* states, the distinct structure of the partial DOS visible in Fig. 6 should be reflected by the partial oxygen densities of states. This is indeed observed in Fig. 7, where we display the contributions from each type of oxygen separately. We have resolved the partial DOS into their three *p* contributions. In order to facilitate the discussion, we complement the figures with Table IV, where we combine those particular V 3*d* and O 2*p* orbitals that, within a molecular orbital picture, are expected to overlap.

Turning to the e_g derived bands first, we mention the double peak structure of the V $3d_{x^2-y^2}$ partial DOS with

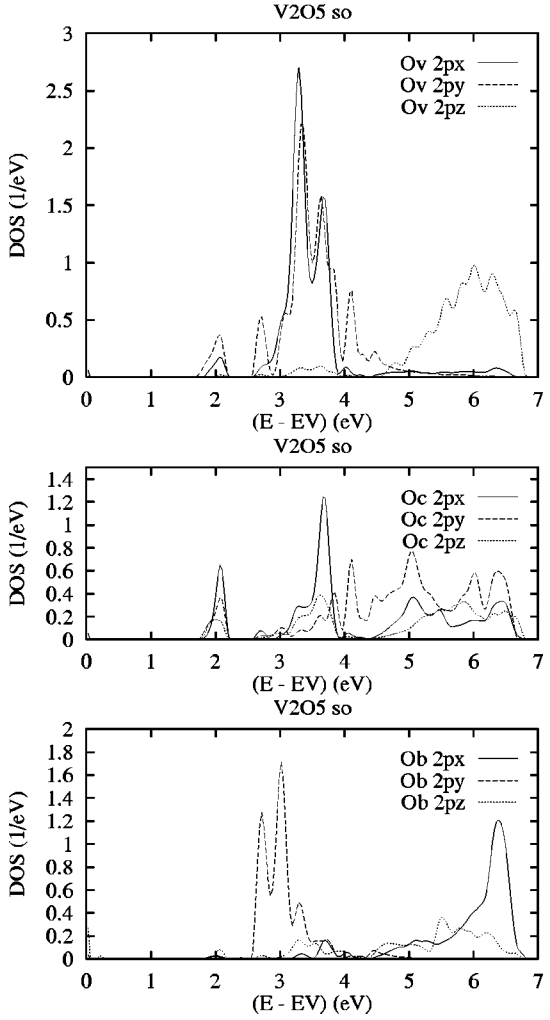

FIG. 7. Partial O $2p$ DOS of V_2O_5.

peaks at 5 and ≈6.3 eV as well as the appearance of the dominant V $3d_{3z^2-r^2}$ contribution in the energy region above ≈5.5 eV. The shape of the V $3d_{x^2-y^2}$ peak around 5 eV resembles that of the O_c $2p_x$ and $2p_y$ DOS and thus indicates the p-d hybridization. The peak at ≈6.3 eV, in contrast, is derived mainly from overlap with the O_b $2p_x$ states and, to a much lesser degree, with the $2p_x$ and $2p_y$ states of the chain oxygen atoms. Still, overlap with the O_c $2p_y$ orbitals is larger than with the $2p_x$ states. The high energy $3d_{3z^2-r^2}$ contribution, finally, originates from strong hybridization with the O_v $2p_z$ states.

For the t_{2g} states, which are responsible for the weaker π type overlap with the oxygen $2p$ states, we observe mainly three features in Fig. 6: (i) the striking double peak in the interval between 3 and 4 eV of both the V $3d_{xz}$ and $3d_{yz}$

TABLE IV. V $3d$-O $2p$ orbital overlaps.

	O_v	O_c	O_b
V $3d_{xy}$		$2p_y$,$2p_x$	$2p_y$
V $3d_{xz}$	$2p_x$	$2p_z$	$2p_z$
V $3d_{yz}$	$2p_y$	$2p_z$	
V $3d_{x^2-y^2}$		$2p_x$,$2p_y$	$2p_x$
V $3d_{3z^2-r^2}$	$2p_z$		

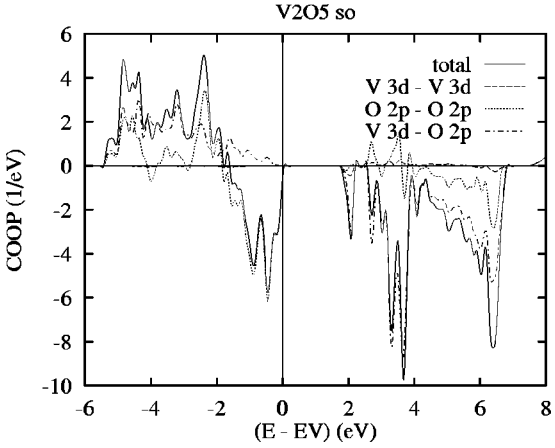

FIG. 8. Total and partial crystal orbital overlap populations (COOP) of V_2O_5.

partial DOS clearly indicates overlap with the O_v $2p_x$ and $2p_y$ orbitals; (ii) the double peak in the energy range from 2.5 to 3.5 eV in the V $3d_{xy}$ partial DOS results from hybridization with the O_b $2p_y$ orbitals; (iii) the peak of the split-off conduction band is due to the V $3d_{xy}$-O_c $2p_x/2p_y$ hybridization.

Of the remaining peaks we point out the $d_{x^2-y^2}$ DOS at about 3 eV. It results from the vertical shifts of the vanadium atoms towards the vanadyl oxygen atoms, which induces a partial π-like overlap of this orbital with the O_v $2p_x$ and $2p_y$ orbitals.

Both the vanadium and oxygen partial DOS thus reflect the peculiarities of the crystal structure. The short V-O_b and, in particular, V-O_v bonds cause an increased bonding-antibonding splitting of the resulting orbitals, hence an upshift of the corresponding antibonding states relative to the valence-band maximum. In reversed order, a similar shift of partial DOS is found in the occupied bonding vanadium-oxygen states where bands with predominantly V $3d_{3z^2-r^2}$-O_v $2p_z$ and V $3d_{x^2-y^2}$-O_b $2p_x$ character appear in the lower half of the valence band. Bands with dominant contributions from the chain oxygen atoms, in contrast, experience a smaller bonding-antibonding splitting due to the larger V-O_c bond length and hence their antibonding bands stay at lower energies. In particular, the relative weakly bound V $3d_{xy}$- O_c $2p_x/2p_y$ derived bands separate from the main part of the unoccupied states and form the split-off conduction band. Our results thus confirm the work of Lambrecht *et al.*, who, by using an effective tight-binding Hamiltonian and symmetry considerations, likewise attributed the split-off band to those V $3d$ and O $2p$ orbitals that have the smallest π-type overlap, hence, the smallest bonding-antibonding splitting.[30]

C. Chemical bonding

We complement the previous discussion by addressing the chemical bonding of V_2O_5 via the crystal orbital overlap population, as shown in Fig. 8. The COOP curves display the rather ''canonical'' behavior, being positive (bonding) and negative (antibonding) in the low and high energy regions of a band, respectively. Whereas the V-V bonding is almost negligible, this canonical trend is visible for the oxygen-oxygen overlap for both the valence and the conduction

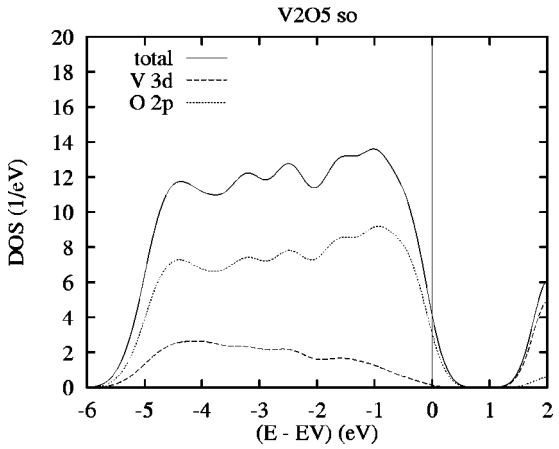

FIG. 9. Total and partial DOS of V_2O_5 folded with a 0.5 eV wide Gaussian.

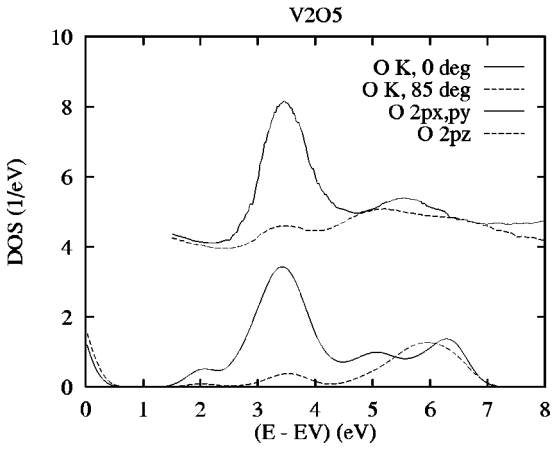

FIG. 11. Partial O $2p$ DOS of V_2O_5 folded with a 0.5 eV wide Gaussian (lower set of curves) and XAS O K edge spectra (upper set of curves; from Ref. 18).

bands separately. The COOP curve resulting from V $3d$-O $2p$ bonding, in contrast, extends from the bottom of the valence band to the top of the conduction band, and changes sign at the valence-band maximum. As a consequence, there are only bonding V $3d$-O $2p$ contributions in the occupied part of the spectrum, whereas antibonding states are shifted to above the band gap. The vanadium-oxygen bonding is thus the decisive factor for the stability of V_2O_5. Note, however, that the low binding part of the valence band appears to be almost V-O nonbonding. This is in accordance with the results of Zhang and Henrich.[15]

D. Comparison to experiment

We display in Figs. 9, 10, and 11 the total and partial V $3d$ and O $2p$ densities of states folded with a Gaussian of 0.5 eV width for the occupied and unoccupied part of the spectrum, respectively. The total DOS in Fig. 9 compares very well with the XPS spectra by Fiermans *et al.*[12] and the UPS spectra by Shin *et al.* as well as by Zhang and Henrich,[14,15] which show an approximately 5.5 eV wide valence band. In the curves given by Zhang and Henrich, the valence band falls into three peaks at about 1.0, 2.5, and 4.5 eV below the valence-band maximum, the relative weights of which, however, are quite sensitive to photon energy.[15] This is in agreement with the spectra displayed by Shin *et al.*, which have two peaks at 0.8 and 2.5 eV, but only a shoulder at 4.3 eV binding energy.[14] The three-peak structure is less marked in the XPS curves. In contrast, these spectra resemble more the form of the V $3d$ partial DOS, which is consistent with the fact that the latter states have a larger cross section in XPS.[14,48]

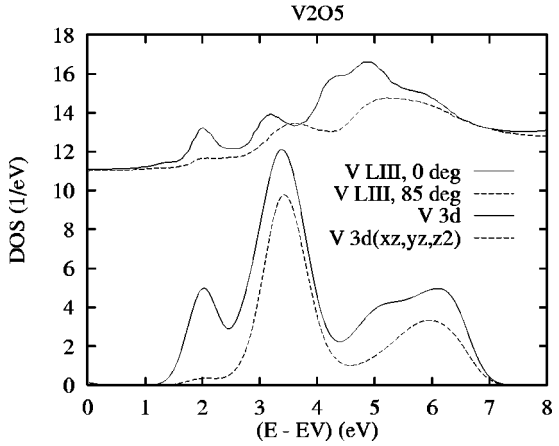

FIG. 10. Partial V $3d$ DOS of V_2O_5 folded with a 0.5 eV wide Gaussian (lower set of curves) and XAS V L_{III} edge spectra (upper set of curves; from Ref. 18).

For the unoccupied states the calculated band positions and widths are in close agreement with those deduced from the optical reflectance data by Mokerov *et al.*[11] In Figs. 10 and 11 we have added soft-x-ray absorption spectra as measured by Goering *et al.*[18] In order to probe the angular dependence, in these experiments the polarization vector **E** was oriented either nearly parallel (ϕ=85°) or else perpendicular (ϕ=0°) to the crystals c axis, which is perpendicular to the (ab) planes. In the former case, dipole selection rules allow for transitions from V $2p$ to the V $3d_{xz}$, $3d_{yz}$, $3d_{3z^2-r^2}$ states and from O $1s$ to the O $2p_z$ state. In contrast, for **E** perpendicular to the c axis, transitions to all five V $3d$ as well as to the O $2p_x$ and $2p_y$ states may occur. We have added the partial DOS of the corresponding final states in Figs. 10 and 11. The agreement between experiment and theory is striking. This holds not only for the positions of the peaks but also for their angular dependence. We point especially to the suppression, on increase of the angle ϕ, of the peak due to the split-off conduction band in Fig. 10 as well as of the O $2p$ peak at 3.4 eV in Fig. 11, which is a consequence of the V $3d_{xy}$-O $2p_x/2p_y$ character of this band. Even smaller details such as, for instance, the double peak structure in the V $3d$ and O $2p_x/2p_y$ DOS above $\approx$ 4 eV (ϕ=0° spectra) and its reduction to a single peak in the spectra for ϕ=85° are described correctly.

E. Role of crystalline distortions

In this section we address the question of why vanadium pentoxide reveals the peculiar quasi-two-dimensional crystal structure as compared to the neighboring $3d^0$ compound, TiO_2, which is a semiconductor with an optical band gap of 3.05 eV and crystallizes in the more regular rutile structure with only one type of oxygen atom and two different Ti-O

TABLE V. Crystal structure parameters of hypothetically idealized V_2O_5.

Atom	Wyckoff positions	Parameters x	y	z
V	$(4f)$	0.08333	0.25	0.0
O_v	$(4f)$	0.08333	0.25	0.5
O_c	$(4f)$	−0.08333	0.25	0.0
O_b	$(2a)$	0.25	0.25	0.0

bond lengths.[34] For this reason we investigate various hypothetical crystal structures for V_2O_5 resulting from an increase of the local symmetry.

From the discussion of the crystal structure given in Sec. II, one might conclude that in the fictitious reference structure both the vertical movements of the vanadium and vanadyl oxygen atoms as well as the lateral displacement of the vanadium and chain oxygen atoms parallel to the x axis should be eliminated. The atoms would then form perfect (ab) planes their z values being either zero or 0.5. Within the planes, the zigzag of the double chains would be eliminated and the x components of the vanadium, vanadyl, and chain oxygen atoms take the values $x(O_b)\pm 1/6$. The crystal structure parameters for the resulting idealized positions of the atoms are listed in Table V. However, the so-constructed idealized crystal structure is based on a simultaneous reduction of both types of displacements and hence does not allow to unambiguously attribute changes of the electronic structure to one of the two modes. For this reason, we proceed in two steps, where we either eliminate the vertical or the lateral displacement. Still, in both cases the resulting crystal structures are artificial. The calculations are performed in complete analogy to those for the ''real'' structure as described in Sec. III. The only difference is that, due to the changes in the atomic positions, different empty sphere positions and sphere radii for all atomic spheres have to be used.[49]

1. Out-of-plane displacements

First, we turn to the vertical shifts and set the z components of all atoms either to zero or 0.5. Note that this actually changes the lattice from simple to base-centered orthorhombic. However, in order to facilitate the subsequent discussion, we will stay with the notions of the simple orthorhombic lattice.

As is seen in Fig. 12, the artificial idealization of the z components leads to a metallic band structure. However, as analysis of the band characters reveals, we are actually dealing with a semimetal where the former valence and conduction bands just share a common energy range of about 0.3 eV width without experiencing additional hybridizations. The partial DOS as shown in Figs. 13 and 14 can be understood in the light of the discussion of Sec. IV B. We observe the strong V d_{xz}/d_{yz} dominated peaks at ≈1 and 1.5 eV as well as the V d_{xy} contributions at ≈0.7 and 1.7 eV. The accompanying oxygen $2p$ partial DOS follow the schematics of the orbital overlaps listed in Table IV.

As compared to the partial DOS of ''real'' V_2O_5 shown in Figs. 6 and 7, we observe a striking broadening of the V d_{xz}, d_{yz}, and $d_{3z^2-r^2}$ derived bands. This causes the enhanced dispersion along the line Γ-Z in the energy range from −3 to 3.5 eV and results from the assumption of equal V-O_v bond lengths. The considerable downshift of these states results from the increase of the shorter of the V-O_v distances. This reduces the overlap between the V d_{xz}/d_{yz} and the O_v $2p_x/2p_y$ orbitals and, hence, the bonding-antibonding splitting. Both the broadening and the downshift cause the finite density of states at E_F. Substantial shifts are also observed below the Fermi energy where the O_v $2p$ states are destabilized and the corresponding occupied bandwidth is reduced from 5.5 to 3 eV. Finally, the downshift of the unoccupied V d_{xy} states can be attributed to the decreasing overlap of the V $3d$ states with the O_v $2p_x/2p_y$ orbitals, which contribute to the split-off conduction band in Fig. 7.

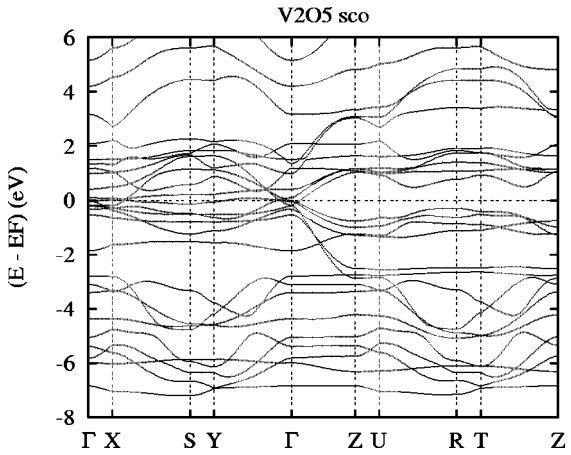

FIG. 12. Electronic bands of hypothetical V_2O_5 with idealized z components along selected symmetry lines.

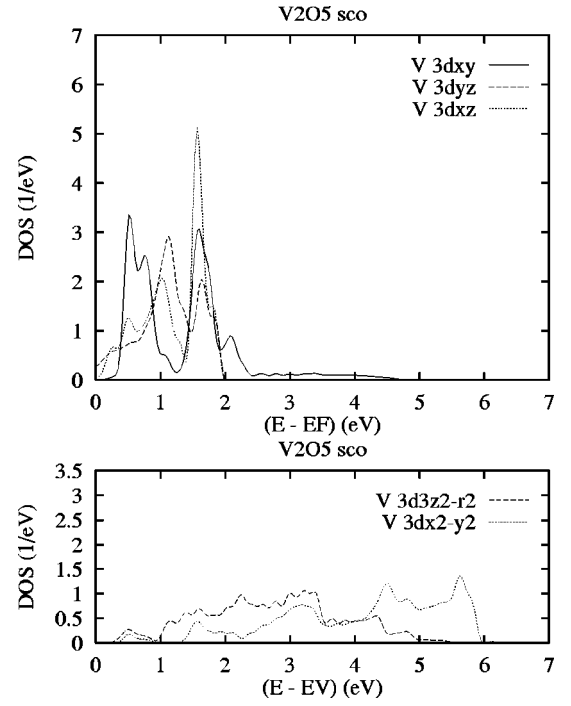

FIG. 13. Partial V $3d$ t_{2g} and e_g DOS of hypothetical V_2O_5 with idealized z components.

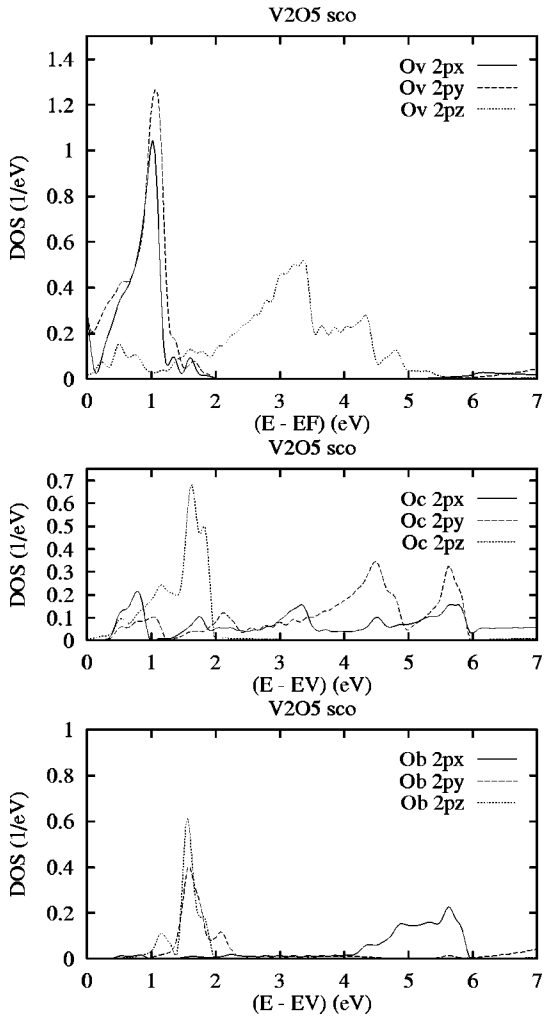

FIG. 14. Partial O $2p$ DOS of hypothetical V_2O_5 with idealized z components.

2. In-plane displacements

The situation is different when we adjust the in-plane projections of the atomic positions while keeping the observed z components. According to the band structure displayed in Fig. 15, this hypothetical V_2O_5 is at the borderline between a semiconductor and a semimetal. However, the increase in

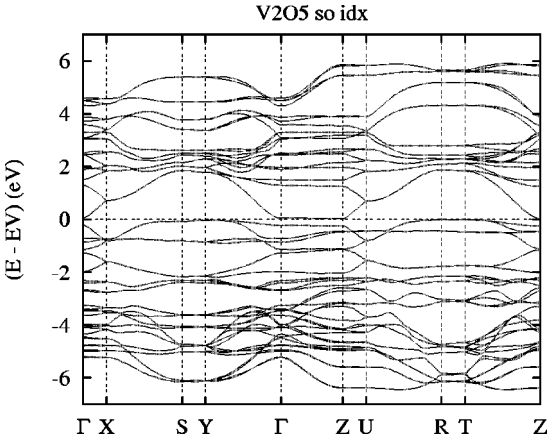

FIG. 15. Electronic bands of hypothetical V_2O_5 with idealized x components along selected symmetry lines.

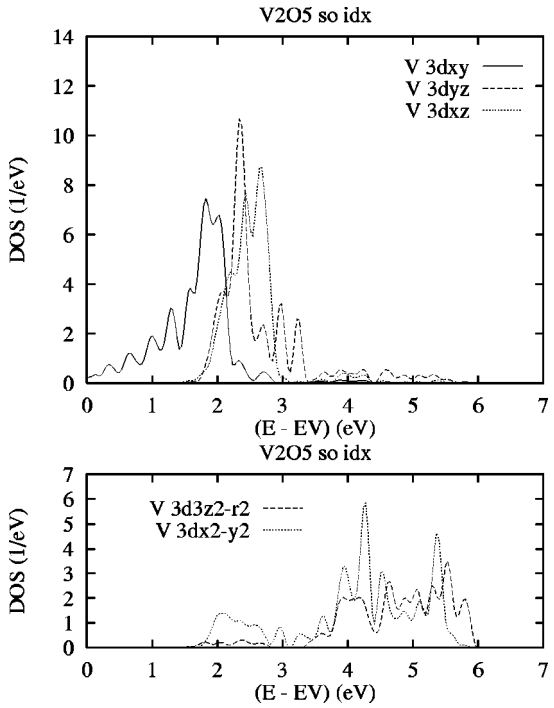

FIG. 16. Partial V $3d$ t_{2g} and e_g DOS of hypothetical V_2O_5 with idealized x components.

dispersion now is along the lines Γ-X and Γ-Y. According to the partial DOS shown in Figs. 16 and 17, the most striking changes are due to the V d_{xy} states. The distance between the peaks at 2 and 3 eV in Fig. 7 has shrunk due to the lateral shifts of the atoms, which make the V-O_c and V-O_b more alike and thereby lead to a comparable bonding-antibonding splitting. At the same time, due to the alignment of the V- O_c double chains, the in-plane dispersion increases substantially. Although the split-off conduction band has a larger width, it is still separated from the higher bands.

Summarizing, the crystal structure of V_2O_5 can be described in terms of two different atomic displacements, which cause distinct changes of the electronic structure. (i) Starting from the idealized reference crystal structure given in Table V, the vertical displacement of the vanadium and vanadyl oxygen atoms increases the overlap between the V d_{xz}/d_{yz} and O_v $2p_x/2p_y$ orbitals and, hence, the corresponding bonding-antibonding splitting. As a consequence, the antibonding V d_{xz}/d_{yz} derived states move up in energy and increase the optical band gap. The bonding O_v $2p_x/2p_y$ dominated states, in contrast, are stabilized, thus lowering the total energy. The latter effect could be explained by the strong V $3d$-O $2p$ hybridization, which has been reported for several vanadium oxides.[18,50,51] (ii) The distortions resulting from the lateral displacement of the vanadium and chain oxygen atoms lead to a drastic decrease of the width of the V $3d_{xy}$ derived split-off conduction band and contribute to the separation of occupied and unoccupied states.

Taken together, both the vertical and lateral displacements, while causing substantial deformations of the octahedra, contribute to the optical band gap and thus lead to the semiconducting ground state of V_2O_5. This is different for TiO_2, where the energy separation of the atomic Ti $3d$ and O $2p$ states is larger from the outset and, hence, leaves enough room for a complete separation between the resulting

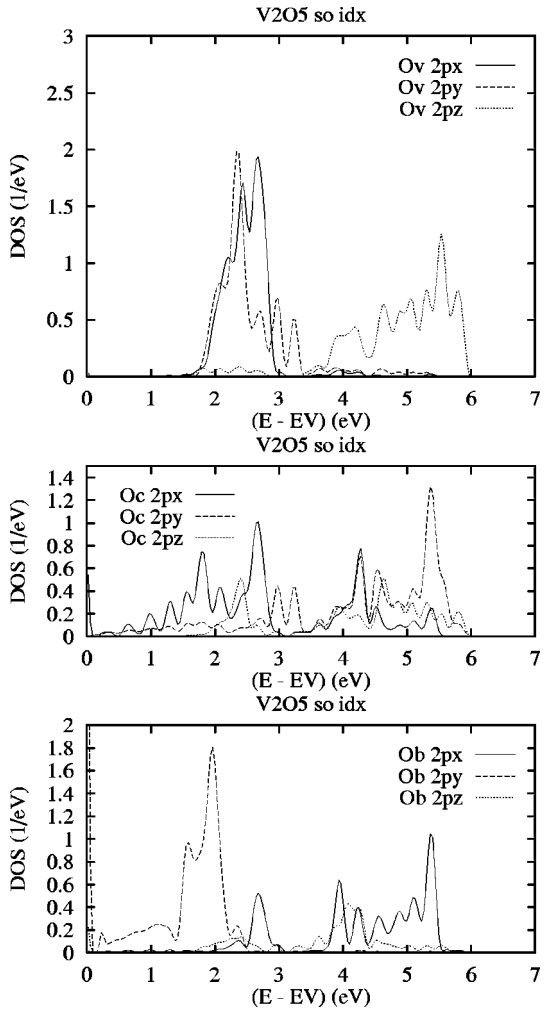

FIG. 17. Partial O $2p$ DOS of hypothetical V_2O_5 with idealized x components.

bonding and antibonding states without the need for additional stabilizing mechanisms.

V. CONCLUSION

In the present work, first-principles ASW calculations were used to describe the electronic properties of vanadium pentoxide. Strong p-d hybridization leads to the formation of an O $2p$ dominated bonding valence band, whereas the conduction band comprises the antibonding states, which mainly derive from crystal field split V $3d$ t_{2g} and, at higher energies, e_g orbitals.

The deviations of the VO_6 octahedra from cubic symmetry cause additional splittings and result in the appearance of a narrow split-off conduction band right above the optical band gap. This originates from weakly bound V $3d_{xy}$ and O_c $2p_x$ orbitals and is responsible for the observed low carrier mobility.

In order to access the role of the striking deformations of the VO_6 octahedra, additional calculations were performed where either the vertical or the lateral displacements of the vanadium atoms were removed. From these simulations we find that the vertical mode predominantly increases the bonding-antibonding splitting of the V $3d_{xz}/3d_{yz}$ derived bands, which stabilizes the compound and increases the optical gap. The lateral mode, in contrast, suppresses the dispersion of the split-off V $3d_{xy}$ conduction band and thus also leads to an increase of the gap. The combination of both modes, finally, enhances the chemical stability and ensures the semiconducting ground state.

ACKNOWLEDGMENTS

We are indebted to S. Horn, U. Eckern, and R. Claessen for many fruitful discussions and a critical reading of the manuscript. Thanks are due to E. Goering for supplying the experimental data. The careful editorial help of C. Wunsch is gratefully acknowledged. This work was supported by the Deutsche Forschungsgemeinschaft (Forschergruppe HO 955/2-1).

APPENDIX: SPHERE GEOMETRY OPTIMIZATION

The muffin-tin approximation (MTA) models the full crystal potential by spherically symmetric potential wells and a constant potential in the remaining interstitial region.[34] A variant of the MTA is the atomic sphere approximation (ASA), which, in addition, requires the spheres to fill all space. Both approximations lay the groundwork for a very efficient determination of the electronic wave function.

For open crystal structures, both the MTA and the ASA are usually extended by the introduction of so-called empty spheres (ES) inside of which the interstitial potential is replaced by a spherically symmetric one.[52] The collection of all, physical and empty, spheres then again leads to an artificially close packed structure. Since the potential resulting from all spherical wells should represent the full crystal potential as closely as possible, it remains a challenge to find, first, optimal empty sphere positions and, second, optimal radii for all spheres.

To achieve an efficient solution of the aforementioned problem, we have developed the sphere geometry optimization (SGO) algorithm, which allows to treat complicated crystal structures and has proven to be very fast.[53] It is based on the observation that the full crystal potential is well approximated by the overlapping free atom potential of the constituent atoms[54] and thus could be used for the selection of ES positions and sphere radii *before* the self-consistent calculation is actually started.[55]

In a first step, the SGO algorithm locates optimal ES positions. Since the ES enter as spherical potential wells, searching for their optimal positions is equivalent to tracing the (local) maxima of the overlapping free atom potential. As an alternative, we implemented a search for the centers of the largest spherical voids. Experience showed that both approaches yield identical results. At the same time, the second method turned out to be much faster than the first one. This way we were able to reduce the problem of locating the ES positions to the standard problem of optimizing a rather simple objective function. Nevertheless, since we are dealing with a highly nonlinear function in a multidimensional space, this optimization still poses a formidable task. Having tested different optimization techniques, we finally opted for using genetic algorithms that have found widespread use in recent years.[56]

Next, the radii of all spheres have to be determined.

Within the ASA, we thus have to search for that set of radii that keeps the overlaps of the spheres small while giving rise to atomic potentials, the superposition of which still resembles the full potential. We have found that the best solution consists of maximizing the volume filled by all spheres while certain overlap limits are enforced. Hence, we have again transformed the problem to a multidimensional optimization procedure, which is accessible to the same means as that mentioned before.

In conclusion, by developing the SGO algorithm we have arrived at an efficient method that supplies an optimal set of empty sphere positions and sphere radii for a subsequent all-electron self-consistent field calculation given only the atomic coordinates.

*Electronic address: eyert@physik.uni-augsburg.de

[1] W. Brückner, H. Oppermann, W. Reichelt, J. I. Terukow, F. A. Tschudnowski, and E. Wolf, *Vanadiumoxide* (Akademie-Verlag, Berlin, 1983).
[2] F. J. Morin, Phys. Rev. Lett. **3**, 34 (1959).
[3] J. Boros, Z. Phys. **126**, 721 (1949).
[4] T. Allersma, R. Hakim, T. N. Kennedy, and J. D. Mackenzie, J. Chem. Phys. **46**, 154 (1967).
[5] A. Bystrom, K. A. Wilhelmi, and O. Brotzen, Acta Chem. Scand. **4**, 1119 (1950).
[6] H. G. Bachmann, F. R. Ahmed, and W. H. Barnes, Z. Kristallogr. **115**, 110 (1961).
[7] H. G. Bachmann and W. H. Barnes, Z. Kristallogr. **115**, 215 (1961).
[8] R. Enhalbert and J. Galy, Acta Crystallogr., Sect. C: Cryst. Struct. Commun. **42**, 1467 (1986).
[9] V. A. Ioffe and I. B. Patrina, Phys. Status Solidi **40**, 389 (1970).
[10] N. Kenny, C. R. Kannewurf, and D. H. Whitmore, J. Phys. Chem. Solids **27**, 1237 (1966).
[11] V. G. Mokerov, V. L. Makarov, V. B. Tulvinskii, and A. R. Begishev, Opt. Spectrosc. **40**, 58 (1976).
[12] L. Fiermans, R. Hoogewijs, and J. Vennik, Surf. Sci. **47**, 1 (1975).
[13] V. M. Cherkashenko, V. E. Dolgikh, and V. L. Volkov, Fiz. Tverd. Tela (Leningrad) **30**, 386 (1988) [Sov. Phys. Solid State **30**, 220 (1988)].
[14] S. Shin, S. Suga, M. Taniguchi, M. Fujisawa, H. Kanzaki, A. Fujimori, H. Daimon, Y. Ueda, K. Kosuge, and S. Kachi, Phys. Rev. B **41**, 4993 (1990).
[15] Z. Zhang and V. E. Henrich, Surf. Sci. **321**, 133 (1994).
[16] E. Goering, O. Müller, M. L. denBoer, and S. Horn, Physica B **194-196**, 1217 (1994).
[17] E. Goering, O. Müller, M. Klemm, J. P. Urbach, H. Petersen, C. Jung, M. L. denBoer, and S. Horn, Physica B **208&209**, 300 (1995).
[18] E. Goering, O. Müller, M. Klemm, M. L. denBoer, and S. Horn, Philos. Mag. B **75**, 229 (1997).
[19] P. A. Carpy and J. Galy, Acta Crystallogr., Sect. B: Struct. Crystallogr. Cryst. Chem. **31**, 1481 (1975).
[20] M. Isobe and Y. Ueda, J. Phys. Soc. Jpn. **65**, 1178 (1996).
[21] Y. Fujii, H. Nakao, T. Yosihama, M. Nishi, K. Nakajima, K. Kakurai, M. Isobe, Y. Ueda, and H. Sawa, J. Phys. Soc. Jpn. **66**, 326 (1997).
[22] T. Ohama, M. Isobe, H. Yasuoka, and Y. Ueda, J. Phys. Soc. Jpn. **66**, 545 (1997).
[23] M. Weiden, R. Hauptmann, C. Geibel, F. Steglich, M. Fischer, P. Lemmens, and G. Güntherodt, Z. Phys. B **103**, 1 (1997).
[24] A. N. Vasil'ev, A. I. Smirnov, M. Isobe, and Y. Ueda, Phys. Rev. B **56**, 5065 (1997).
[25] T. Yosihama, M. Nishi, K. Nakajima, K. Kakurai, Y. Fujii, M. Isobe, and Y. Ueda, Physica B **234-236**, 539 (1997).
[26] M. Lohmann, A. Loidl, M. Klemm, G. Obermeier, and S. Horn, Solid State Commun. **104**, 649 (1997).
[27] W. Lambrecht, B. Djafari-Rouhani, M. Lannoo, and J. Vennik, J. Phys. C **13**, 2485 (1980).
[28] W. Lambrecht, B. Djafari-Rouhani, M. Lannoo, P. Clauws, L. Fiermans, and J. Vennik, J. Phys. C **13**, 2503 (1980).
[29] D. W. Bullett, J. Phys. C **13**, L595 (1980).
[30] W. Lambrecht, B. Djafari-Rouhani, and J. Vennik, J. Phys. C **14**, 4785 (1981).
[31] A. Michalak, M. Witko, and K. Hermann, Surf. Sci. **375**, 385 (1997).
[32] R. Hoffmann, *Solids and Surfaces: A Chemist's View of Bonding in Extended Structures* (VCH, New York, 1988).
[33] V. Eyert and S. F. Matar (unpublished).
[34] V. Eyert, *Electronic Structure Calculations for Crystalline Materials*, in *Density Functional Methods: Applications in Chemistry and Materials Science*, edited by M. Springborg (Wiley, Chichester, 1997), pp. 233-304.
[35] M. Schramme, R. Barth, V. Eyert, E. Goering, O. Müller, and S. Horn, Verh. Dtsch. Phys. Ges. **32**, O18.7 (1997).
[36] M. Schramme, R. Barth, V. Eyert, E. Goering, O. Müller, S. Horn, and M. L. denBoer, Bull. Am. Phys. Soc. **42**, 138 (1997).
[37] M. Schramme, R. Barth, V. Eyert, E. Goering, O. Müller, K.-H. Höck, S. Horn, and M. L. denBoer (unpublished).
[38] P. Hohenberg and W. Kohn, Phys. Rev. **136**, B864 (1964).
[39] W. Kohn and L. J. Sham, Phys. Rev. **140**, A1133 (1965).
[40] A. R. Williams, J. Kübler, and C. D. Gelatt, Jr., Phys. Rev. B **19**, 6094 (1979).
[41] D. D. Koelling and B. N. Harmon, J. Phys. C **10**, 3107 (1977).
[42] H. Gollisch and L. Fritsche, Phys. Status Solidi B **86**, 145 (1978).
[43] J. Kübler and V. Eyert, *Electronic Structure Calculations*, in *Electronic and Magnetic Properties of Metals and Ceramics*, edited by K. H. J. Buschow (VCH Verlagsgesellschaft, Weinheim, 1992), pp. 1–145, Vol. 3A of the series *Materials Science and Technology*, edited by R. W. Cahn, P. Haasen, and E. J. Kramer (VCH Verlagsgesellschaft, Weinheim, 1991–1996).
[44] V. Eyert, Ph.D. thesis, Technische Hochschule Darmstadt, 1991.
[45] O. K. Andersen, Phys. Rev. B **12**, 3060 (1975).
[46] O. K. Andersen, A. P. Postnikov, and S. Yu. Savrasov, *The Muffin-Tin Orbital Point of View*, in *Applications of Multiple Scattering Theory to Materials Science*, edited by W. H. Butler, P. H. Dederichs, A. Gonis, and R. L. Weaver, MRS Symposia Proceedings No. 253 (Materials Research Society, Pittsburgh, 1992), p. 37.
[47] V. Eyert, J. Comput. Phys. **124**, 271 (1996).
[48] J. J. Yeh and I. Lindau, At. Data Nucl. Data Tables **32**, 1 (1985).
[49] V. Eyert and K.-H. Höck (unpublished).
[50] O. Müller, E. Goering, J. P. Urbach, T. Weber, H. Paulin, M. Klemm, M. L. denBoer, and S. Horn, J. Phys. IV **7**, C2-533 (1997).

[51] R. Zimmermann, R. Claessen, F. Reinert, P. Steiner, and S. Hüfner (unpublished).
[52] J. Keller, J. Phys. C **4**, L85 (1971).
[53] V. Eyert, Hahn-Meitner-Institute Report B548, Berlin, 1997.
[54] L. F. Mattheiss, Phys. Rev. **133**, A1399 (1964).
[55] O. Jepsen and O. K. Andersen, Z. Phys. B **97**, 35 (1995).
[56] D. E. Goldberg, *Genetic Algorithms in Search, Optimization, and Machine Learning* (Addison-Wesley, Reading, 1989).